01 May 2000

FDTD Modeling of Lumped Ferrites

Min Li

Xiao Luo

James L. Drewniak
Missouri University of Science and Technology, drewniak@mst.edu

Recommended Citation

M. Li et al., "FDTD Modeling of Lumped Ferrites," *IEEE Transactions on Electromagnetic Compatibility*, vol. 42, no. 2, pp. 142-151, Institute of Electrical and Electronics Engineers (IEEE), May 2000.
The definitive version is available at https://doi.org/10.1109/15.852408

FDTD Modeling of Lumped Ferrites

Min Li, Xiao Luo, and James L. Drewniak, *Member, IEEE*

***Abstract*—Implementing ferrites in finite-difference time-domain (FDTD) modeling requires special care because of the complex nature of the ferrite impedance. Considerable computational resources and time are required to directly implement a ferrite in the FDTD method. Fitting the ferrite impedance to an exponential series with the generalized-pencil-of-function (GPOF) method and using recursive convolution is an approach that minimizes the additional computational burden. An FDTD algorithm for a lumped ferrite using GPOF and recursive convolution is presented herein. Two different ferrite impedances in a test enclosure were studied experimentally to demonstrate the FDTD modeling approach. The agreement is generally good.**

***Index Terms*—FDTD, ferrite, GPOF.**

I. Introduction

NUMERICAL modeling is a common approach for developing insight and EMC design directions. FDTD is one method used extensively because it is straightforward and simple to incorporate lumped elements and subcellular modeling. It is of concern to implement ferrites in numerical modeling, since they are often used in high-speed digital designs to mitigate EMI problems. However, incorporating a ferrite in FDTD modeling is difficult because of the complexity of the ferrite frequency response. Special treatment is required to develop an efficient method for modeling ferrites in the FDTD method. Considerable work has been done on incorporating the ferrite behavior through the electromagnetic field interactions [1]–[3], i.e., the magnetic flux density vector $\vec{B}$ is related to the magnetic field vector $\vec{H}$ via a frequency dependent permeability tensor $\vec{\mu}$. This relation is then transformed to the time domain and introduced into Maxwell's equations. Usually, a recursive approach is applied to reduce the required computational resources associated with convolution. Other modeling of ferrites in the FDTD method is through the supplement of Gilbert's equation of motion, which describes the interaction between the magnetic field $\vec{H}$ and the magnetization vector $\vec{M}$ in a magnetized ferrite in the time domain [4]–[8], or through the incorporation of a frequency-dependent magnetic susceptibility [9], [10]. Most of this previous work is on ferrite materials that span a number of FDTD cells. Small-size lumped element ferrites are extensively used in printed circuit board (PCB) designs as well as for EMI suppression on connector pins and cables.

Manuscript received November 2, 1998; revised December 14, 1999. This work was supported by the EMI Consortium at the University of Missouri-Rolla.

M. Li was with the University of Missouri-Rolla, Rolla, MO 65409–02499 USA. He is now with Lucent Technologies, Princeton, NJ 08542 USA.

X. Luo was with the University of Missouri-Rolla, Rolla, MO 65409–02499 USA. He is now with Lucent Technologies, Norcross, GA 30071 USA.

J. L. Drewniak is with the Department of Electrical Engineering, University of Missouri-Rolla, Rolla, MO 65409–02499 USA.

Publisher Item Identifier S 0018-9375(00)04680-9.

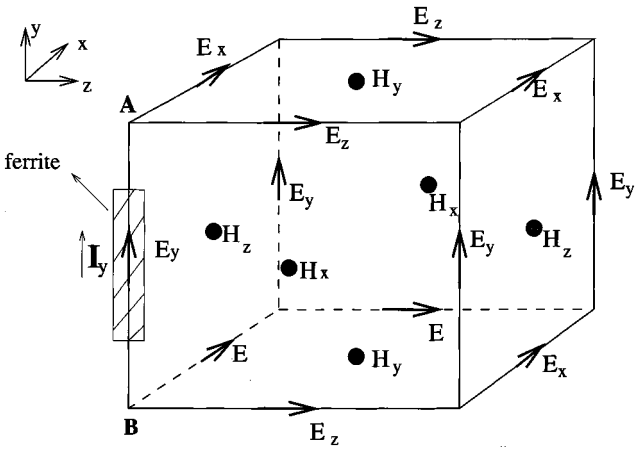

Fig. 1. FDTD modeling of a ferrite as a lumped element.

Work on a ferrite, which is smaller than an FDTD cell size and can be deemed as a lumped element, is limited to modeling it as an *RLC* circuit [11]. An accurate implementation of a lumped ferrite in FDTD is necessary for modeling at the PCB, connector, and cabling levels. It can also be useful to incorporate a lumped ferrite in time-domain multiconductor transmission-line (MTL) modeling [12]. An FDTD algorithm using the generalized-pencil-of-function (GPOF) method and recursive convolution is developed herein for lumped, unsaturated ferrites, and demonstrated experimentally in particular for surface-mount (SMT) ferrites. In the applications herein, the hysteresis is assumed to be negligible. The SMT's are incorporated in the FDTD modeling as lumped elements since their sizes are usually small compared to the FDTD cells. The FDTD results using the algorithm are compared with measured results in a shielding enclosure geometry and generally compare well.

II. FDTD Algorithm for a Lumped Ferrite

The subcellular ferrite algorithm is developed by transforming the frequency-domain ferrite impedance to a time-domain response, then incorporating the time-domain response into the FDTD modeling through an impressed current. GPOF and recursive convolution are used to minimize the computational burden in the time-marching scheme. Specifically, the procedure entails:

- obtaining the frequency-domain ferrite impedance from measurements or a data sheet;
- inverse fast Fourier transforming (IFFT) to get the time-domain ferrite response from the frequency-domain impedance;
- extracting a finite sum of complex exponential terms using GPOF to express the time-domain response;

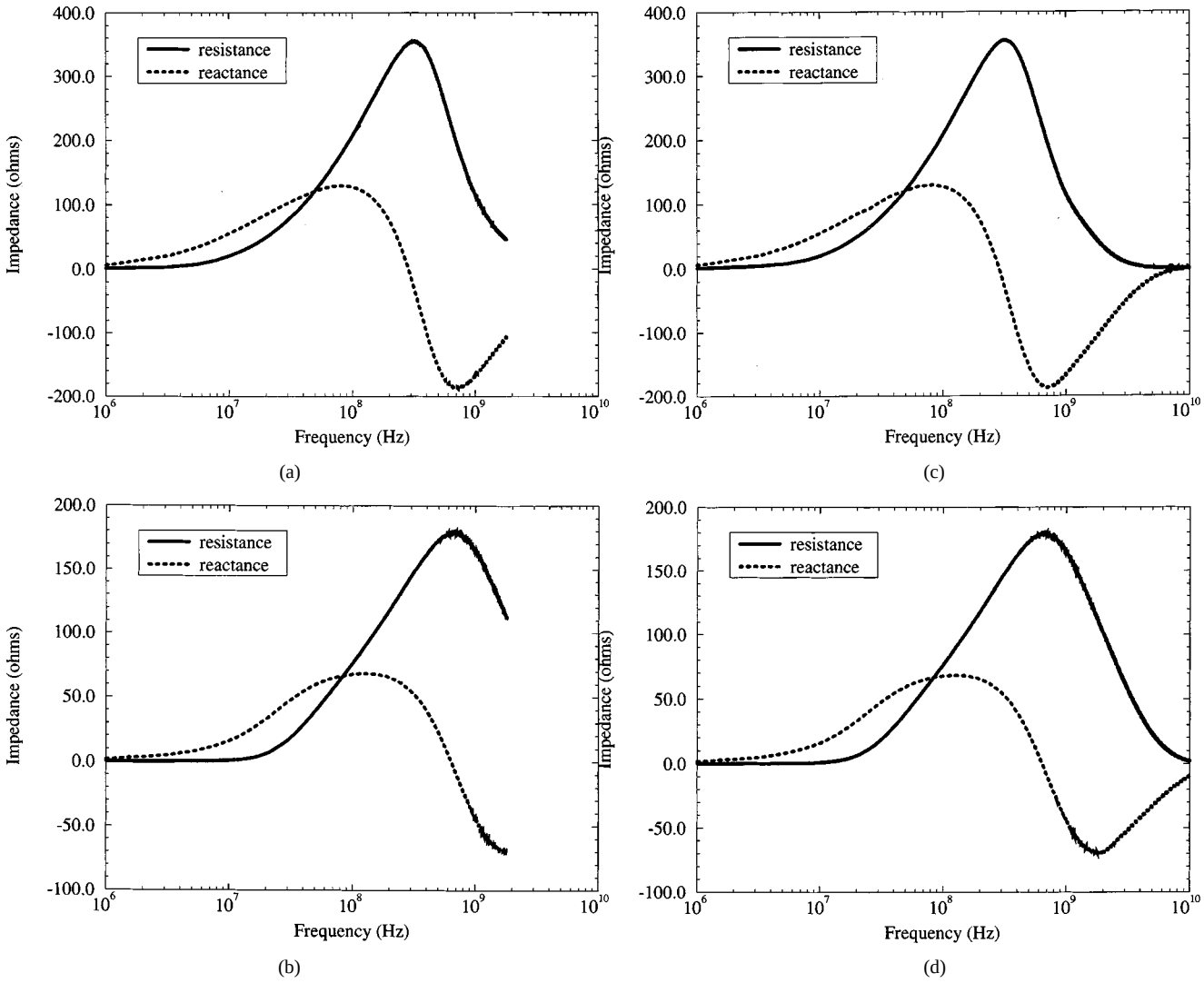

Fig. 2. Measured resistance and reactance for (a) Ferrite 1 and (b) Ferrite 2 and extended resistance and reactance for (c) Ferrite 1 and (d) Ferrite 2.

- modifying the complex exponential terms to correspond to the time increment of the FDTD modeling (which usually is not the same as the time interval obtained from the sampling in the frequency-domain);
- incorporating the ferrite time-domain response into the FDTD updating equations through an impressed current;
- using recursive convolution with the complex exponential terms of the ferrite time response and a complex supplementary function;
- decomposing the complex exponential terms and the supplementary function into real and imaginary parts, which are updated separately;
- implementing the final FDTD updating equation using the real or imaginary parts of the complex exponential terms and the supplementary function.

The frequency-domain response of a ferrite impedance can be obtained from the manufacturer's data sheet or measurements with an impedance analyzer. The corresponding frequency for the mth frequency data point is $m \times \Delta f$ where Δf is the frequency discretization increment. The IFFT is then employed to obtain the time-domain response of the ferrite impedance from the frequency-domain information. The frequency data is then further extended to $2N$ by conjugating the first N steps in order to get a real time response after the IFFT, i.e.,

$$\tilde{T}(m) = \tilde{T}^*(2N+1-m), \qquad m = N+1, \cdots, 2N \quad (1)$$

where the tilde denotes a frequency-domain quantity. The resulting time response from the IFFT should be causal because the ferrite is physically a causal convergent filter [13]. However, the causality may be violated due to experimental error in characterizing the ferrite impedance. The time-domain response at time steps less than zero is ignored because it is usually much smaller than that at time steps greater than zero. The time-domain response of the ferrite impedance is $T^{\text{ferr}}(n)$ for time steps $n = 1, \cdots, 2N$ and the time interval is $\Delta t = 1/(2N \times \Delta f)$.

The time response $T^{\text{ferr}}(n)$ is then incorporated in the FDTD modeling through an impressed current relating the voltage and current in the FDTD cell where the lumped ferrite is located. A recursive formulation by means of GPOF is also utilized to reduce the required computational burden. First, a finite sum of complex exponential terms to express the time response

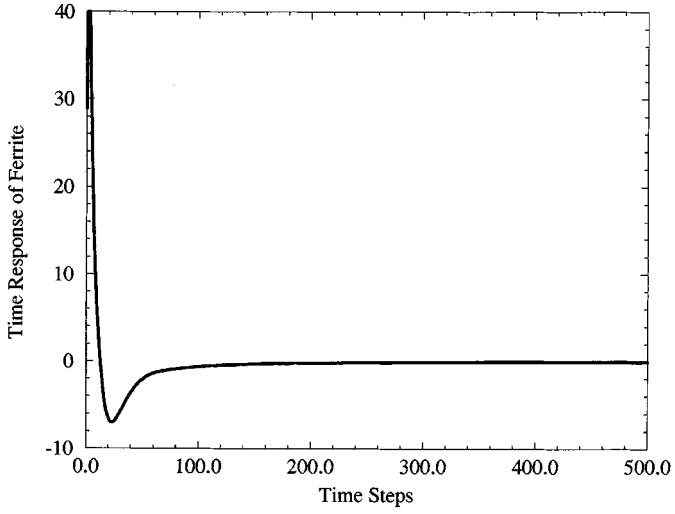

(a)

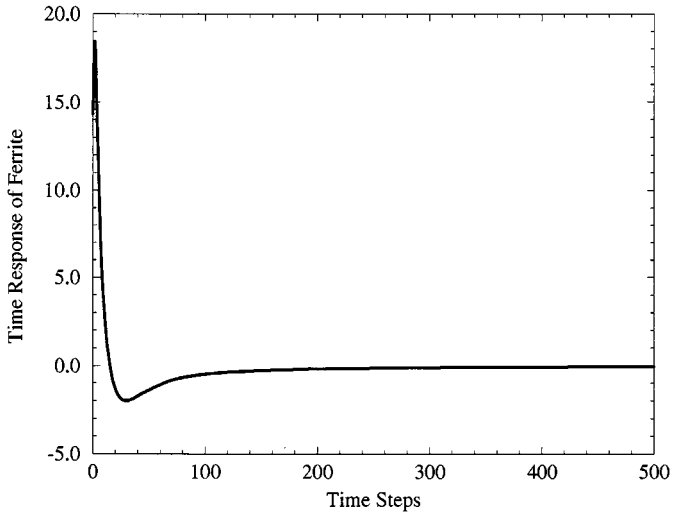

(b)

Fig. 3. Calculated time response for: (a) Ferrite 1 and (b) Ferrite 2.

$T^{\text{ferr}}(n)$ is obtained. GPOF is used to extract these terms [14]. A sum of M terms is used as

$$T^{\text{ferr}}(n) = \sum_{\ell=1}^{M} R_\ell^{\text{ferr}} \left(e^{-\alpha_\ell + j\omega_\ell}\right)^n = \sum_{\ell=1}^{M} R_\ell^{\text{ferr}} \left(Z_\ell^{\text{ferr}}\right)^n \quad (2)$$

where α_ℓ, ω_ℓ, R_ℓ^{ferr}, and Z_ℓ^{ferr} are the terms obtained by the GPOF method, and R_ℓ^{ferr} and Z_ℓ^{ferr} are generally complex. The time increment is $\Delta t = 1/(2N \times \Delta f)$, from the previous IFFT calculation. However, the time increment in the FDTD modeling is dt, which usually is not equal to Δt, requiring a modification of the complex exponential terms due to different sampling increments in the time domain

$$R_\ell = R_\ell^{\text{ferr}} \frac{dt}{\Delta t} \quad (3)$$

$$Z_\ell = \left(Z_\ell^{\text{ferr}}\right)^{dt/\Delta t}. \quad (4)$$

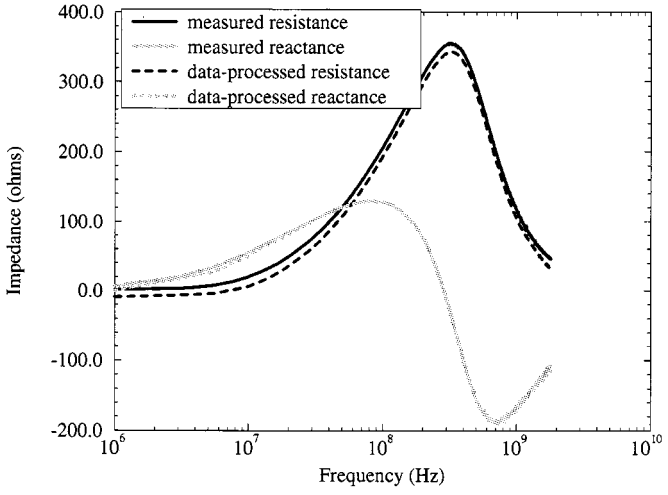

(a)

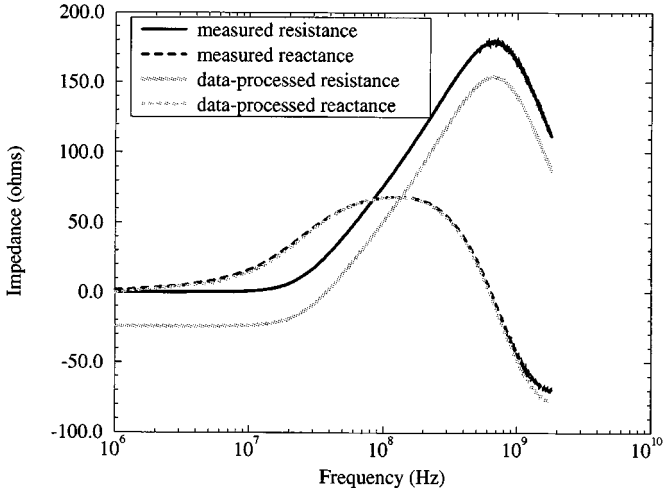

(b)

Fig. 4. Comparison between the measured and data-processed impedance for: (a) Ferrite 1 and (b) Ferrite 2.

It can then be shown that approximately the same frequency response is obtained as

$$\begin{aligned}
\tilde{T}'(f) &= \sum_{m=0}^{\infty} \sum_{\ell=1}^{M} R_\ell Z_\ell^m e^{-jm2\pi dtf} \\
&= \sum_{m=0}^{\infty} \sum_{\ell=1}^{M} \frac{dt}{\Delta t} R_\ell^{\text{ferr}} \left(Z_\ell^{\text{ferr}}\right)^{(dt/\Delta t)m} \\
&\quad \cdot e^{-j\Delta t 2\pi (dt/\Delta t) mf} \\
&= \sum_{\ell=1}^{M} \sum_{m'=0,(dt/\Delta t),2(dt/\Delta t),\cdots}^{\infty} \frac{dt}{\Delta t} R_\ell^{\text{ferr}} \left(Z_\ell^{\text{ferr}}\right)^{m'} \\
&\quad \cdot e^{-j\Delta t 2\pi m' f} \\
&\approx \sum_{\ell=1}^{M} \frac{1}{\Delta t} \int_0^{\infty} R_\ell^{\text{ferr}} \left(Z_\ell^{\text{ferr}}\right)^x e^{-j\Delta t 2\pi x f}\, dx \\
&\approx \sum_{\ell=1}^{M} \frac{1}{\Delta t} \sum_{n=0}^{\infty} R_\ell^{\text{ferr}} \left(Z_\ell^{\text{ferr}}\right)^n e^{-j\Delta t 2\pi n f} \Delta t \\
&= \sum_{n=0}^{\infty} \sum_{\ell=1}^{M} R_\ell^{\text{ferr}} \left(Z_\ell^{\text{ferr}}\right)^n e^{-j\Delta t 2\pi n f} \\
&= \tilde{T}(f) \quad (5)
\end{aligned}$$

where the time increment dt is small with respect to the functional variation in the integral between the sum and integral to satisfy the approximation, which is satisfied herein.

The time-domain response of the ferrite impedance at time step n (time interval of dt) in the FDTD modeling is then

$$T_z(n) = \sum_{\ell=1}^{M} R_\ell Z_\ell^n. \tag{6}$$

The FFT result of $T_z(n)$ for a time interval of dt then gives nearly the same frequency response as that of $T^{\text{ferr}}(n)$ for time interval of Δt. The parameters R_ℓ and Z_ℓ are then used in the following development of the lumped ferrite algorithm.

The ferrite time-domain response obtained above can be implemented in the FDTD modeling through an impressed current I since lumped element ferrites are of concern here. The ferrite is assumed oriented along the y-direction and placed at the position of E_y in the FDTD cell (i, j, k), shown in Fig. 1. The i, j, and k are the FDTD cell indexes along the x, y, and z directions, respectively. The updating equation for E_y at time step $n+1$ based on its value at the previous time step n, circulating magnetic field components H_x and H_z, and the impressed current I is [15]

$$\begin{aligned} &E_{yi,j,k}(n+1) \\ &\quad = E_{yi,j,k}(n) + \frac{dt}{\epsilon}\left[\frac{H_{xi,j,k}\left(n+\frac{1}{2}\right) - H_{xi,j,k-1}\left(n+\frac{1}{2}\right)}{dz}\right. \\ &\qquad \left. - \frac{H_{zi,j,k}\left(n+\frac{1}{2}\right) - H_{zi-1,j,k}\left(n+\frac{1}{2}\right)}{dx}\right] \\ &\qquad - \frac{dt}{\epsilon}\left[\frac{I\left(n+\frac{1}{2}\right)}{dzdx}\right] \end{aligned} \tag{7}$$

where ϵ is the permittivity and dx, dz are the FDTD cell dimensions along the x and z directions. The impressed current I is related to E_y through the voltage across the ferrite by $V = E_y \times dy$ and the ferrite response T_z in the time domain by the discrete convolution

$$V(n) = \sum_{p=0}^{n} T_z(p) I(n-p) \tag{8}$$

where $V(n)$ is the voltage across the ferrite at time step n. At time-step $n+1$

$$\begin{aligned} V(n+1) &= \sum_{p=0}^{n+1} T_z(p) I(n+1-p) \\ &= \sum_{p=0}^{n} T_z(p) I(n+1-p) + T_z(n+1) I(0) \end{aligned} \tag{9}$$

where the last term is zero since $I(0) = 0$ (the initial condition in the FDTD modeling). Using a semi-implicit approximation gives

$$\frac{V(n)+V(n+1)}{2} = \sum_{p=0}^{n} Tz(p) \frac{I(n-p)+I(n+1-p)}{2} \tag{10}$$

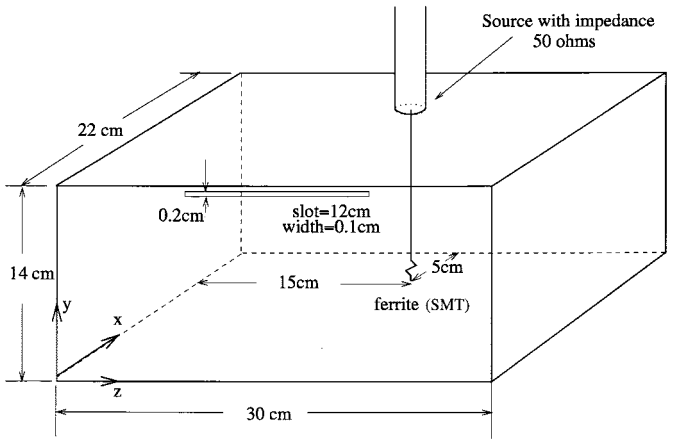

Fig. 5. The geometry of the shielding enclosure for the measurements and FDTD modeling.

or

$$V\left(n+\frac{1}{2}\right) = \sum_{p=0}^{n} T_z(p) I\left(n+\frac{1}{2}-p\right) \tag{11}$$

where the value of V and I at time step $n+(1/2)$ is obtained as the average of the values at time steps n and $n+1$.

The sum in (11) requires all the I values at the previous time steps, and in general can consume an inordinate amount of computational resources and time. The M terms of the exponential sum in (6) are employed in (11) to obtain the recursive updating

$$\begin{aligned} V\left(n+\frac{1}{2}\right) &= \sum_{p=0}^{n}\sum_{\ell=1}^{M} R_\ell Z_\ell^p I\left(n+\frac{1}{2}-p\right) \\ &= \sum_{\ell=1}^{M}\sum_{p=0}^{n} R_\ell Z_\ell^p I\left(n+\frac{1}{2}-p\right) \end{aligned} \tag{12}$$

which is shown in Appendix A to be

$$V\left(n+\frac{1}{2}\right) = \sum_{\ell=1}^{M} R_\ell I\left(n+\frac{1}{2}\right) + \sum_{\ell=1}^{M} \phi_\ell(n) \tag{13}$$

where $I(n+(1/2))$ is not a function of the index ℓ and $\phi_\ell(n)$ is updated as

$$\phi_\ell(n) = R_\ell Z_\ell I\left(n-\frac{1}{2}\right) + Z_\ell \phi_\ell(n-1). \tag{14}$$

Further data processing is again required since the constants R_ℓ and Z_ℓ are generally complex. It is shown in Appendix B that the real and complex parts of the function $\phi_\ell(n)$ can be updated separately and the updating equation for $V(n+(1/2))$ can be rewritten as

$$V\left(n+\frac{1}{2}\right) = \sum_{\ell=1}^{M'} 2[R_\ell]^{\text{real}} I\left(n+\frac{1}{2}\right) + \sum_{g=1}^{M'} 2[\phi_\ell(n)]^{\text{real}} \tag{15}$$

where M' is the number of conjugate pairs plus any real terms for the exponential sums in (6). $I(n+(1/2))$ can be expressed with $V(n+(1/2))$ from (15) as

$$I\left(n+\frac{1}{2}\right) = \frac{V^{n+(1/2)} - \sum_{\ell=1}^{M'} 2[\phi_\ell(n)]^{\text{real}}}{\sum_{\ell=1}^{M'} 2[R_\ell]^{\text{real}}}. \tag{16}$$

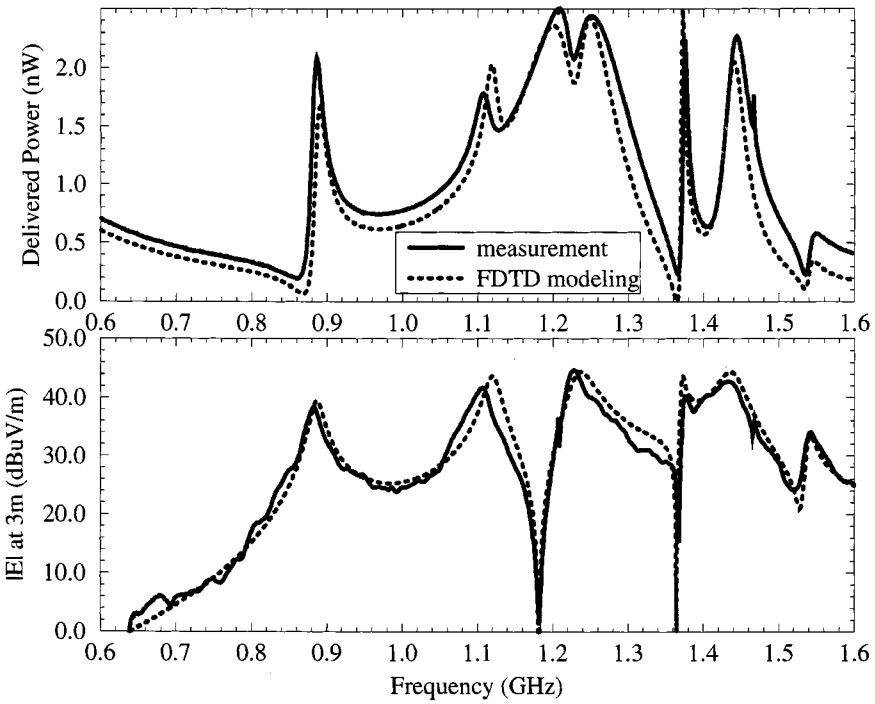

Fig. 6. Comparison between measurements and FDTD modeling of the delivered power and electric field strength 3 m away for the enclosure configuration with Ferrite 1.

Equation (16) is then used in the FDTD update (7) to get the ferrite lumped-element equation for E_y at time step $n+1$ as shown in (17), where $\phi_\ell(n)^{\text{real}}$ is updated as in (B.9) and (B.10) in Appendix B.

III. Experimental Corroboration

The FDTD procedure detailed above for a lumped ferrite was implemented and the results compared with measurements in a shielding enclosure configuration. Two surface mount (SMT) ferrites with package sizes 1.6 mm × 0.8 mm and 4.5 mm × 1.6 mm, denoted Ferrite 1 and Ferrite 2, respectively, were measured with an HP 4291A impedance analyzer with an HP16192A SMT test fixture over the frequency range from 1 to 1800 MHz. The number of measured data points over the frequency range was 801, thus, the sampling interval was $\Delta f = (1800-1)/800 = 2.249$ MHz. The measured resistance and reactance are shown in Fig. 2(a) and (b) for Ferrite 1 and Ferrite 2, respectively. The frequency of the magnitude peak for Ferrite 1 was approximately 250 MHz and the resistance peak value was 360 Ω. The frequency of the magnitude peak for Ferrite 2 was approximately 700 MHz and the resistance peak value was 180 Ω.

The frequency response information was not complete because the upper frequency of the measurements was limited to 1.8 GHz by the upper band limit of the impedance analyzer. Since the complete frequency response was required in the IFFT, the GPOF method was also employed to extrapolate the higher frequency responses [14]. This was not a part of the ferrite algorithm, but rather an extrapolation of information. The total number of data points was extrapolated to $N = 1600$ for Ferrite 1 and $N = 3200$ for Ferrite 2, as shown in Fig. 2(c) and (d), respectively. For Ferrite 2, it was difficult to apply the Matrix Pencil method directly to the reactance since the magnitude of the reactance was still increasing at the upper frequency 1.8 GHz. Some decreasing points were artificially

$$E_y(n+1) = \left\{ \left(1 - \frac{dt\,dy}{2\epsilon\,dx\,dz \sum_{\ell=1}^{M'} R_\ell^{\text{real}}} \right) E_y(n) + \frac{dt \sum_{\ell=1}^{M'} 2[\phi_\ell(n)]^{\text{real}}}{\epsilon\,dx\,dz \sum_{\ell=1}^{M'} R_\ell^{\text{real}}} + \frac{dt}{\epsilon} \left[\frac{H_{xi,j,k}\left(n+\frac{1}{2}\right) - H_{xi,j,k-1}\left(n+\frac{1}{2}\right)}{dz} - \frac{H_{zi,j,k}\left(n+\frac{1}{2}\right) - H_{zi-1,j,k}\left(n+\frac{1}{2}\right)}{dx} \right] \right\} \Bigg/ \left(1 + \frac{dt\,dy}{2\epsilon\,dx\,dz \sum_{\ell=1}^{M'} R_\ell^{\text{real}}} \right) \tag{17}$$

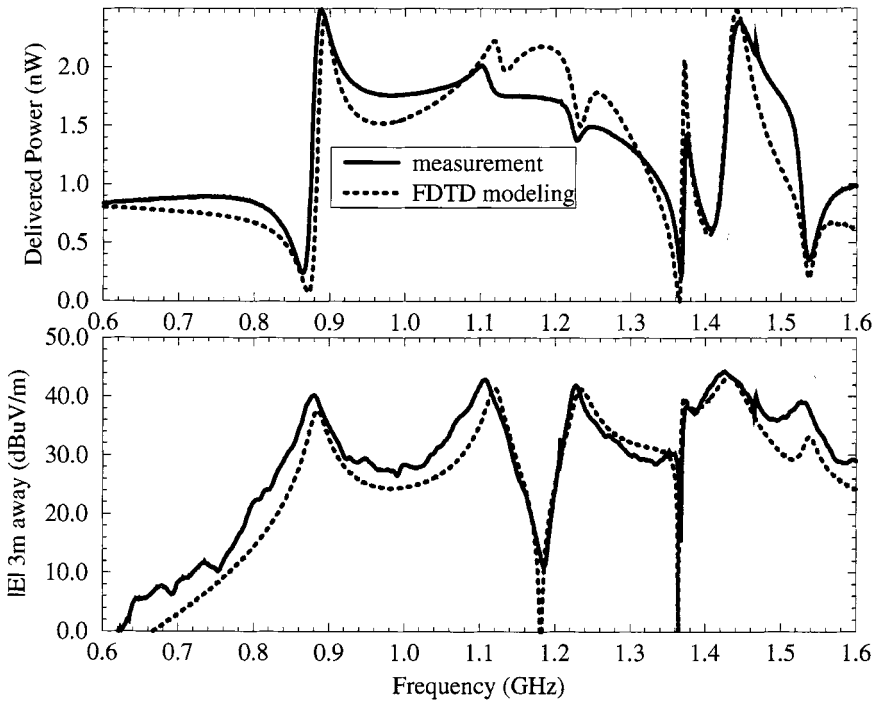

Fig. 7. Comparison between measurements and FDTD modeling of the delivered power and electric field strength 3 m away for the enclosure configuration with Ferrite 2.

introduced above 1.8 GHz before the GPOF was applied in order to achieve convergence in the algorithm. Inaccuracy due to the artificially added data points inevitably resulted and could be avoided with a measurement extended to higher frequencies. However, the available HP 4291A instrument had an upper frequency limit of 1.8 GHz.

The IFFT was applied to obtain the time-domain responses for Ferrite 1 and Ferrite 2. The time-response at time steps less than zero was ignored because it was noncausal, and resulted from measurement errors. The peak of the time-response at time steps less than zero was generally one fifth of that at time steps larger than zero. The time-domain response for Ferrite 1 and Ferrite 2 are shown in Fig. 3(a) and (b), respectively. The shapes of the time responses were similar for both ferrites, with the late time responses approaching zero. To study the effect of the incomplete data, GPOF extrapolation, and IFFT in the last step, an FFT was applied to the resulting real and causal time-domain responses to compare the transformed frequency-domain ferrite impedance with the measurements. The resulting comparisons for Ferrite 1 and Ferrite 2 are shown in Fig. 4(a) and (b), respectively. The agreement for Ferrite 1 is good, while the discrepancy for Ferrite 2 is about 20% for the resistance peak value, due to the artificially added points in the reactance as a consequence of incomplete measurements through the rapidly changing part of the ferrite response. The effect of the IFFT was not significant if complete measurements (adequate for the GPOF extrapolation) were available.

Measurements using Ferrite 1 and Ferrite 2 in an enclosure were made in order to assess the accuracy of the proposed ferrite subcellular algorithm in FDTD modeling. The geometry of the experimental conducting enclosure is shown in Fig. 5. The cavity was fed with a 50-Ω coaxial cable probe through a type-N bulkhead connector, which was peripherally bonded to the cavity. The center conductor of the probe was extended to span the width of the cavity with a 0.16-cm-diameter wire and terminated on the opposite cavity wall with an SMT ferrite soldered to a 1.5 in $\times$ 1.5 in square of conductive adhesive copper tape. The feed probe was located at $x = 17$ cm, $y = 14$ cm, $z = 15$ cm. The inside dimensions of the enclosure were 22 cm $\times$ 14 cm $\times$ 30 cm. One-inch copper tape with conductive adhesive was used to electromagnetically seal the seams on the enclosure interior. A 12 cm $\times$ 0.1 cm slot near one corner was employed as the radiator. The case without the slot was obtained by sealing the slot with copper tape. The frequency range of the measurements was 600 MHz to 1.6 GHz in order to excite several cavity modes, slot modes, and the feed-probe TEM mode.

A Wiltron 37 247A network analyzer was employed to measure the reflection coefficient $|S_{11}|$ with Port 1 connected to the feed probe of the enclosure. The real power delivered to the enclosure by the source was calculated from the $|S_{11}|$ measurements as

$$P = \frac{V_s^2}{8Z_0}\left(1 - |S_{11}|^2\right) \tag{18}$$

where Z_0 is the 50-Ω characteristic impedance of the connecting cables and source impedance and V_s is the source voltage, which is normalized to 1 mV, and used in the FDTD modeling. The power available from the source is then 2.5 nW. The radiated field in an anechoic chamber was also measured. The transmission coefficient $|S_{21}|$ was measured with a biconical-log periodic receiving antenna 3 m away connected to Port 2 of the network analyzer. $|S_{21}|$ is related to the electric field strength 3 m away by the antenna factor of the receiving antenna as [16]

$$|E_{3m}| = AF \times |S_{21}| \times V_1 \tag{19}$$

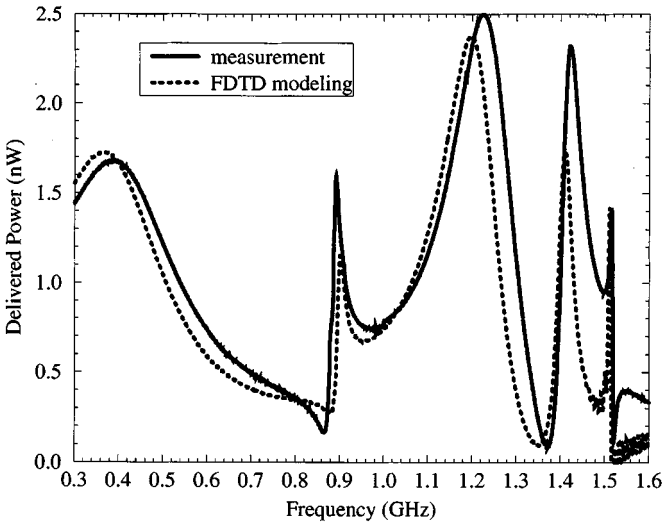

(a)

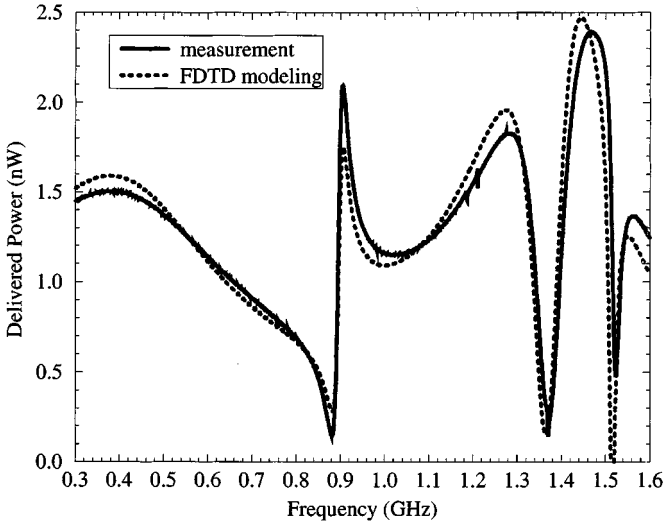

(b)

Fig. 8. Comparison between measurements and FDTD modeling for the enclosure configuration without the slot for (a) Ferrite 1 and (b) a 360 Ω resistor terminating the feed probe.

where AF is the antenna factor of the receiving antenna, and V_1 is the incident voltage from Port 1, which is 0.5 mV for the normalized 1-mV source with a 50-Ω source impedance.

A cell size of 1.0 cm × 0.5 cm × 1.0 cm was employed in the FDTD modeling, where finer discretization along the y direction was used in order to better model the spatial extent of the SMT ferrite terminating the feed probe. Aluminum plates were modeled with perfect electric conducting surfaces by setting the tangential electric field to zero on the cavity walls. The feed probe was modeled by a simple voltage source $V_s = 1$ mV, with a 50-Ω resistance incorporated into a single cell at the feed point. The ferrite was modeled as a lumped element using the algorithm described above. The number of complex exponentials M, was 12 and 13 and the number of conjugate pairs plus real terms M', for the exponential sums was 8 and 9 for Ferrite 1 and Ferrite 2, respectively. The magnetic fields circling the source and ferrite were modeled in the same fashion as a thin wire to give the cross section of the source and ferrite specified physical dimensions [17], [18]. The slot was modeled with the C-TSF thin-slot subcellular algorithm [18], [19] and PML absorbing boundary conditions were employed for the three-dimensional simulations [20]. The PML absorbing layers were eight cells away from the enclosure.

The results for the delivered power and electric field strength 3 m away for Ferrite 1 as the terminating element, with the 12 cm slot as the radiator are shown in Fig. 6. The agreement between the measurements and FDTD modeling is good. The resonances can be identified as cavity-mode resonances and resonances due to the slot [18]. Radiation from cavity-mode resonances, and resonances due to the slot coincided with the delivered power. The discrepancy between the measured and FDTD results at 1.47 GHz is experimental error resulting from a feed probe that was not strictly along the y direction, thus unintended cavity modes were experimentally excited.

The results on the delivered power and electric field strength 3 m away for Ferrite 2 as the terminating element, with the 12 cm slot as the radiator, are shown in Fig. 7. The measurements and FDTD modeling generally agree, but not as well as that of Ferrite 1 due to incomplete frequency-domain impedance information of Ferrite 2. For the delivered power, the maximum discrepancies were around 1.2 GHz, e.g., the frequency at which the ferrite impedance peaks and the cavity half-wavelength window frequency (at this frequency the cavity can be treated as a transmission line with the feed probe as the center conductor [21]). In the modeling, the frequency response of Ferrite 2 obtained from the data processing, shown in Fig. 4(a), was generally lower than the actual frequency response. Thus, the resistance of Ferrite 2 in the modeling was closer to the match of 50 Ω than it actually was. At the half-wavelength windowing frequency, more power was delivered to the enclosure in the FDTD modeling, as seen in Fig. 4(a). The comparison between measurements and modeling for the electric field strength at 3 m is good.

The electric field strengths 3 m away in the above configurations of Ferrite 1 and Ferrite 2 are similar because the radiation mechanism was dominated by the enclosure and slot. Thus, the E field at 3 m is not a severely discriminating criteria for the ferrite model. In order to focus on the ferrite effect, the slot in the enclosure was sealed. The results for Ferrite 1 as the termination without the slot are shown in Fig. 8(a). A 360 Ω resistor [the resistance value at the peak for Ferrite 1, shown in Fig. 2(c)] was utilized in place of the ferrite to compare the above ferrite model and a simple resistor. The results for the delivered power with the 360 Ω resistor termination are shown in Fig. 8(b). The agreement between the measurements and FDTD modeling is generally good. The difference between the ferrite model and resistor model is significant. The recursive ferrite model is more suitable for modeling the ferrite, especially at low frequencies below 500 MHz and frequencies around 1.2 GHz.

The results for delivered power with Ferrite 2 as the terminating element without the slot are shown in Fig. 9(a). A 180 Ω resistor (the resistance value at the peak) was also utilized in place of Ferrite 2. The measured and modeling results are shown in Fig. 9(b). The difference between these two models is significant and the recursive model for a ferrite is more suitable than a resistor at most of the frequencies.

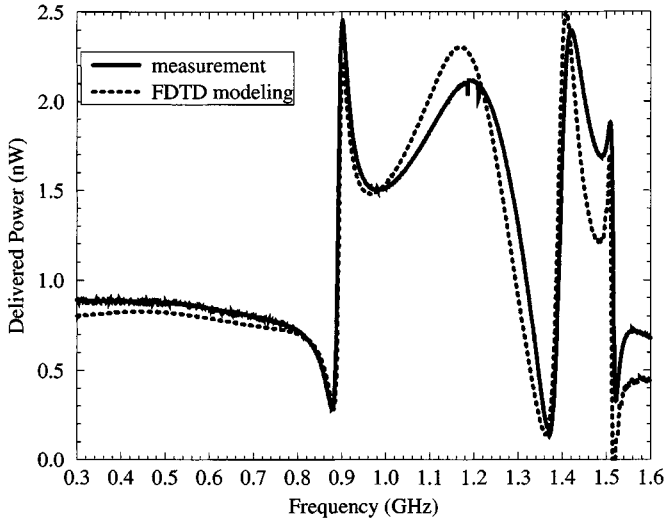

(a)

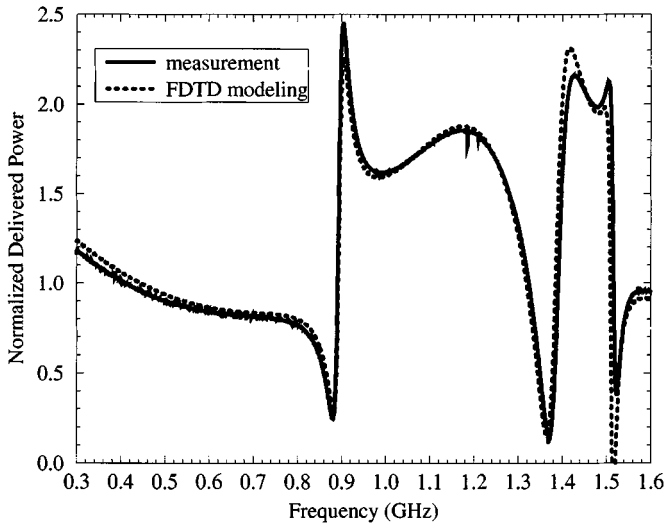

(b)

Fig. 9. Comparison between measurements and FDTD modeling for the enclosure configuration without the slot for (a) Ferrite 2 and (b) a 180-Ω resistor terminating the feed probe.

The phase of S_{11} was also compared to further test the ferrite model. The results of $\angle S_{11}$ for Ferrite 1 terminating the feed wire with no slot in the enclosure are shown in Fig. 10(a), and the results of $\angle S_{11}$ for the 180 Ω resistor are shown in Fig. 10(b). Again, the difference is significant, and the recursive ferrite model is more suitable than a resistor model for a lumped ferrite.

IV. Summary and Conclusion

A lumped ferrite was modeled in FDTD through an impressed current using a recursive convolution formulation. Measurements in a shielding enclosure, which was fed with a wire probe terminated by a ferrite, were made to corroborate the FDTD modeling results. The agreement was generally good. This algorithm is suitable for lumped ferrites and useful in PCB and MTL modeling.

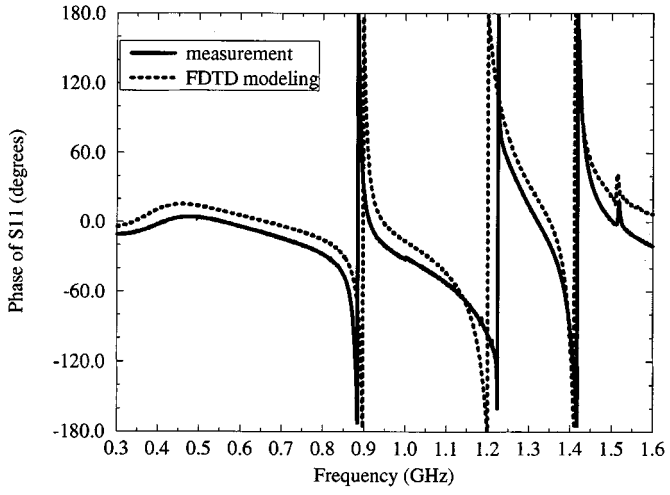

(a)

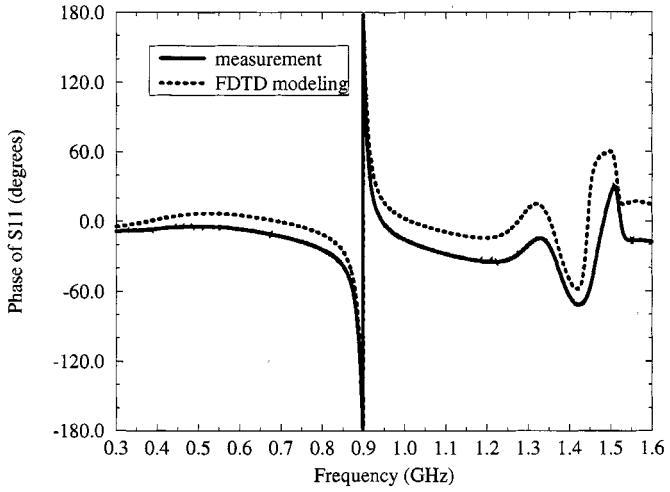

(b)

Fig. 10. Comparison of $\angle S_{11}$ between measurements and FDTD modeling for the enclosure configuration without the slot for (a) Ferrite 1 and a (b) 360-Ω resistor terminating the feed probe.

Appendix A

The time-domain response of a ferrite is actually a discrete-time filter, with the current I at different time steps as the input, and the voltage V as the output. Its recursive convolution can be obtained from the following steps. For $n = 1$

$$\begin{aligned} V\left(\frac{3}{2}\right) &= \sum_{\ell=1}^{M} \sum_{p=0}^{1} R_\ell Z_\ell^p I\left(\frac{3}{2} - p\right) \\ &= \sum_{\ell=1}^{M} \left[R_\ell I\left(\frac{3}{2}\right) + R_\ell Z_\ell I\left(\frac{1}{2}\right) \right] \\ &= \sum_{\ell=1}^{M} \left[R_\ell I\left(\frac{3}{2}\right) + \phi_\ell(1) \right] \end{aligned} \tag{A.1}$$

where $\phi_\ell(1)$ is defined as $\phi_\ell(1) = R_\ell Z_\ell I(1/2)$. And, for $n = 2$

$$V\left(\frac{5}{2}\right) = \sum_{\ell=1}^{M} \sum_{p=0}^{2} R_\ell Z_\ell^p I\left(\frac{5}{2} - p\right)$$

$$= \sum_{\ell=1}^{M} \left[R_\ell I\left(\frac{5}{2}\right) + R_\ell Z_\ell I\left(\frac{3}{2}\right) + R_\ell Z_\ell^2 I\left(\frac{1}{2}\right) \right]$$
$$= \sum_{\ell=1}^{M} \left[R_\ell I\left(\frac{5}{2}\right) + \phi_\ell(2) \right] \quad \text{(A.2)}$$

where $\phi_\ell(2)$ is defined as $\phi_\ell(2) = R_\ell Z_\ell I(3/2) + Z_\ell \phi_\ell(1)$. At the time step n

$$V\left(n+\frac{1}{2}\right) = \sum_{\ell=1}^{M} \sum_{p=0}^{n} R_\ell Z_\ell^p I\left(n+\frac{1}{2}-p\right)$$
$$= \sum_{\ell=1}^{M} \left[R_\ell I\left(n+\frac{1}{2}\right) + \phi_\ell(n) \right] \quad \text{(A.3)}$$

where $\phi_\ell(n)$ is updated by

$$\phi_\ell(n) = R_\ell Z_\ell I\left(n-\tfrac{1}{2}\right) + Z_\ell \phi_\ell(n-1). \quad \text{(A.4)}$$

Appendix B

The ferrite time-domain response $T_z(n)$ is real. Then for each term in the exponential series, with complex constants R_ℓ and Z_ℓ, there are always conjugate terms $R_{\ell'}$ and $Z_{\ell'}$ ($R_{\ell'} = R_\ell^*$, $Z_{\ell'} = Z_\ell^*$), otherwise the constants R_ℓ and Z_ℓ are real. The conjugate pair can be combined to obtain the new updating equations for ϕ_ℓ. Let $R_\ell = c_1 + jc_2$, $R_{\ell'} = c_1 - jc_2$, $Z_\ell = z_1 + jz_2$, and $Z_{\ell'} = z_1 - jz_2$, the update at the first time step is

$$\begin{aligned}\phi_\ell(1) &= (c_1 + jc_2)(z_1 + jz_2) I\left(\tfrac{1}{2}\right) \\ &= (c_1 z_1 - c_2 z_2) I\left(\tfrac{1}{2}\right) + j(c_1 z_2 + c_2 z_1) I\left(\tfrac{1}{2}\right) \\ &= \Re(R_\ell Z\ell) \times I\left(\tfrac{1}{2}\right) + j \times \Im(R_\ell Z\ell) \times I\left(\tfrac{1}{2}\right) \quad \text{(B.1)} \\ \phi_{\ell'}(1) &= (c_1 - jc_2)(z_1 - jz_2) I\left(\tfrac{1}{2}\right) \\ &= (c_1 z_1 - c_2 z_2) I\left(\tfrac{1}{2}\right) - j(c_1 z_2 + c_2 z_1) I\left(\tfrac{1}{2}\right) \\ &= \Re(R_\ell Z\ell) \times I\left(\tfrac{1}{2}\right) - j \times \Im(R_\ell Z\ell) \times I\left(\tfrac{1}{2}\right) \quad \text{(B.2)}\end{aligned}$$

where the constants $\Re(R_\ell Z\ell) = c_1 z_1 - c_2 z_2$ is the real part of $R_\ell Z_\ell$ and $\Im(R_\ell Z\ell) = c_1 z_2 + c_2 z_1$ is the imaginary part. Then let

$$[\phi_\ell(1)]^{\text{real}} = \Re \times I\left(\tfrac{1}{2}\right) \quad \text{(B.3)}$$
$$[\phi_\ell(1)]^{\text{imag}} = \Im(R_\ell Z\ell) \times I\left(\tfrac{1}{2}\right) \quad \text{(B.4)}$$
$$[\phi_\ell(1)] = [\phi_{\ell'}(1)]^*. \quad \text{(B.5)}$$

At time step n

$$\begin{aligned}\phi_\ell(n) &= (c_1 + jc_2)(z_1 + jz_2) I\left(n-\tfrac{1}{2}\right) + (z_1 + jz_2)\phi_\ell(n-1) \\ &= \Re(R_\ell Z\ell) \cdot I\left(n-\tfrac{1}{2}\right) + j \cdot \Im(R_\ell Z\ell) I\left(n-\tfrac{1}{2}\right) \\ &\quad + z_1[\phi_\ell(n-1)]^{\text{real}} - z_2[\phi_\ell(n-1)]^{\text{imag}} \\ &\quad + jz_2[\phi_\ell(n-1)]^{\text{real}} + jz_1[\phi_\ell(n-1)]^{\text{imag}}. \quad \text{(B.6)}\end{aligned}$$

So the real and imaginary part of the function $\phi_\ell(n)$ can be updated independently as

$$[\phi_\ell(n)]^{\text{real}} = \Re(R_\ell Z\ell) \cdot I\left(n-\tfrac{1}{2}\right) + z_1[\phi_\ell(n-1)]^{\text{real}} - z_2[\phi_\ell(n-1)]^{\text{imag}} \quad \text{(B.7)}$$
$$[\phi_\ell(n)]^{\text{imag}} = \Im(R_\ell Z\ell) \cdot I\left(n-\tfrac{1}{2}\right) + z_1[\phi_\ell(n-1)]^{\text{imag}} + z_2[\phi_\ell(n-1)]^{\text{real}}. \quad \text{(B.8)}$$

For the conjugate term, the corresponding ϕ'_ℓ is updated as

$$[\phi_{\ell'}(n)]^{\text{real}} = \Re(R_\ell Z\ell) \cdot I\left(n-\tfrac{1}{2}\right) + z_1[\phi_{g'}(n-1)]^{\text{real}} - z_2[\phi_{g'}(n-1)]^{\text{imag}} \quad \text{(B.9)}$$

$$[\phi_{\ell'}(n)]^{\text{imag}} = \Im(R_\ell Z\ell) \cdot I\left(n-\tfrac{1}{2}\right) + z_1[\phi_{\ell'}(n-1)]^{\text{imag}} + z_2[\phi_{\ell'}(n-1)]^{\text{real}}. \quad \text{(B.10)}$$

It can be shown that $\phi_\ell(n)$ and $\phi_{\ell'}(n)$ are conjugates of each other. The updating (13) for $V(n+(1/2))$ can then be rewritten as

$$\begin{aligned}V\left(n+\tfrac{1}{2}\right) &= \sum_{\ell=1}^{M'} (R_\ell + R'_\ell) I\left(n+\tfrac{1}{2}\right) + \sum_{\ell=1}^{M'} [\phi_\ell(n) + \phi'_\ell(n)] \\ &= \sum_{\ell=1}^{M'} 2[R_\ell]^{\text{real}} I\left(n+\tfrac{1}{2}\right) + \sum_{g=1}^{M'} 2[\phi_\ell(n)]^{\text{real}} \quad \text{(B.11)}\end{aligned}$$

where M' is the number of conjugate pairs for the exponential sums in (6). If R_ℓ and Z_ℓ are real, they can be deemed as conjugates to themselves, resulting in the new conjugate pair of $(R_\ell/2,\ Z_\ell)$ and $(R_\ell/2,\ Z_\ell)$.

Acknowledgment

The authors gratefully acknowledge the use of Sun Microsystems 3-m chamber for making radiated measurements.

References

[1] A. Taflove, *Advances in Computational Electrodynamics: The Finite-Difference Time-Domain Method*. Boston, MA: Artech House, 1998.

[2] K. S. Kunz and R. J. Luebbers, *The Finite Difference Time Domain Method for Electromagnetics*. Boca Raton, FL: CRC, 1993.

[3] T. Monediere, K. B. Pichavant, F. Marty, P. Gelin, and F. Jecko, "FDTD treatment of partically magnetized ferrites with a new permeability tensor model," *IEEE Trans. Microwave Theory Tech.*, vol. 46, pp. 983–986, July 1998.

[4] J. A. Pereda, L. A. Vielva, M. A. Solano, A. Vegas, and A. Prieto, "FDTD analysis of magnetized ferrites: Application to the calculation of dispersion characteristic of ferrite-loaded waveguide," *IEEE Trans. Microwave Theory Tech.*, vol. 43, pp. 350–356, Feb. 1995.

[5] R. Holland, "Finite-difference time-domain (FDTD) analysis of magnetic diffusion," *IEEE Trans. Electromagn. Compat.*, vol. 36, pp. 32–39, Feb. 1994.

[6] M. Okoniewski, "FDTD analysis of magnetized ferrites: A more efficient algorithm," *IEEE Microwave Guided Wave Lett.*, vol. 4, pp. 169–171, June 1994.

[7] J. A. Pereda, L. A. Vielva, and A. Prieto, "A treatment of magnetized ferrites using the FDTD method," *IEEE Microwave Guided Wave Lett.*, vol. 3, pp. 136–138, May 1993.

[8] J. A. Pereda, L. A. Vielva, A. Vegas, and A. Prieta, "FDTD analysis of magnetized ferrites: An approach based on the rotated Richtmyer difference scheme," *IEEE Microwave Guided Wave Lett.*, vol. 3, pp. 322–324, Sept. 1993.

[9] C. L. Holloway, P. McKenna, and D. A. Steffen, "Finite-difference time-domain modeling for field predictions inside rooms," in *Proc. IEEE Electromagn. Compat. Symp.*, Austin, TX, Aug. 1997, pp. 60–65.

[10] C. L. Holloway, P. McKenna, and R. T. Hohnk, "The effects of gaps in ferrite tiles on both absorber and chamber performance," in *Proc. IEEE Electromagn. Compat. Symp.*, Seattle, WA, Aug. 1999, pp. 239–244.

[11] C. W. Lam, "Finite-difference time-domain analysis of common-mode cable currents," in *Annu. Rev. Progress Appl. Comput. Electromagn.*, vol. 2, Monterey, CA, 1996, pp. 870–876.

[12] C. R. Paul, *Analysis of Milticonductor Transmission Lines*. New York: Wiley, 1994.

[13] J. G. Proakis and D. G. Manolakis, *Digital Signal Processing Principles, Algorithms, and Applications*. New York: Macmillan, 1992.
[14] T. K. Sarkar and O. Pereira, "Using the matrix pencil method to estimate the parameters of a sum of complex exponentials," *IEEE Trans. Antennas Propagat. Mag.*, vol. 37, pp. 48–54, Feb. 1995.
[15] Y.-S. Tsuei, A. C. Cangellaris, and J. L. Prince, "Rigorous electromagnetic modeling of chip-to-package (first-level) interconnections," *IEEE Trans. Comp. Hybrids Manuf. Technol.*, vol. 16, pp. 876–882, Dec. 1993.
[16] D. Morgan, *A Handbook for Testing and Measurement*. Stevenage, U.K.: Peter Peregrinus Ltd., 1994.
[17] D. M. Hockanson, J. L. Drewniak, T. H. Hubing, and T. P. Van Doren, "FDTD modeling of common-mode radiation from cables," *IEEE Trans. Electromagn. Compat.*, vol. 38, pp. 376–387, Aug. 1996.
[18] M. Li, K.-P. Ma, J. L. Drewniak, T. H. Hubing, and T. P. Van Doren, "Numerical and experimental corroboration of an FDTD thin-slot model for slots near corners of shielding enclosures," *IEEE Trans. Electromagn. Compat.*, vol. 39, pp. 225–232, Aug. 1997.
[19] J. Gilbert and R. Holland, "Implementation of the thin-slot formalism in the finite-difference EMP code THREDII," *IEEE Trans. Nucl. Sci.*, vol. NS-28, pp. 4269–4274, Dec. 1981.
[20] J. P. Berenger, "Perfectly matched layer for the absorption of electromagnetic waves," *J. Comput. Phys.*, vol. 114, pp. 185–200, Oct. 1994.
[21] M. Li, "Investigation of electromagnetic interference through slots in shielding enclosures: Finite-difference time-domain simulations and experiments," M.S. thesis, Univ. Missouri-Rolla, 1996.

Min Li was born in China in 1968. She received the B.S. (honors) and M.S. (honors) degrees in physics from Fudan University, Shanghai, China, in 1990 and 1993, respectively, and the M.S. and Ph.D. degrees in electrical engineering from the University of Missouri-Rolla, in 1996 and 1999, respectively.

Since 1995, she has studied and worked in the Electromagnetic Compatibility Laboratory, University of Missouri-Rolla. Her research interests include numerical and experimental study of electromagnetic compatibility problems. She is currently with Lucent Technologies. She was supported by a Dean's fellowship and assistantship in her research and studies.

Dr. Li was the winner of the 1998 IEEE EMC Society President Memory Award.

Xiao Luo was born in China, in 1969. She received the B.S. degree from the Chinese South Institute of Technologies, Shanghai, China, and the M.S. degree from the Fudan University, Shanghai, China, in 1990 and 1993, respectively, both in physics, and the M.S. degree in electrical engineering from the University of Missouri-Rolla, in 1998.

Since 1996, she has studied and worked in the Electromagnetic Compatibility Laboratory, University of Missouri-Rolla. Her research interests include numerical and experimental study of electromagnetic compatibility problems. She is currently with Lucent Technologies, Shanghai.

James L. Drewniak (S'85–M'90) received the B.S. (highest honors), M.S., and Ph.D. degrees in electrical engineering from the University of Illinois, Urbana-Champaign, in 1985, 1987, and 1991, respectively.

He joined the Electrical Engineering Department, University of Missouri-Rolla, in 1991, where he is part of the Electromagnetic Compatibility Laboratory. His research interests include the development and application of numerical methods for investigating electromagnetic compatibility problems, packaging effects, and antenna analysis, as well as experimental studies in electromagnetic compatibility and antennas.